Chemical Physics Letters 639 (2015) 151–156

Contents lists available at ScienceDirect

Chemical Physics Letters

journal homepage: www.elsevier.com/locate/cplett

A combined ab initio and Franck–Condon simulation study of the photodetachment spectra of the $HCBr^-$ anion

Zhen-li Yang[a], Ya-juan Feng[b], Jun Liang[a,**], Wei Huang[b,*]

[a] Institute of Atomic and Molecular Physics, College of Physics and Electronic Information, Anhui Normal University, Wuhu 241000, PR China
[b] Laboratory of Atmospheric Physico-Chemistry, Anhui Institute of Optics and Fine Mechanics, Chinese Academy of Sciences, Hefei, Anhui 230031, PR China

ARTICLE INFO

Article history:
Received 16 July 2015
In final form 10 September 2015
Available online 18 September 2015

ABSTRACT

Geometry optimization and harmonic vibrational frequency calculations have been performed on the $\tilde{X}^2A''$ state of $HCBr^-$, and $\tilde{X}^1A'$ and $\tilde{a}^3A''$ states of HCBr. The term energy and electron affinity of HCBr were calculated and extrapolated to the complete basis set limit. The Duschinsky matrix and displacement vector were calculated at the CCSD(T)/aug-cc-pVQZ level. The normal mode mixing effects played a minor role and can be neglected for the $HCBr(\tilde{X}^1A')$–$HCBr^-(\tilde{X}^2A'')$ photodetachment. Spectral simulations involved the $HCBr(\tilde{X}^1A')$–$HCBr^-(\tilde{X}^2A'')$ and $HCBr(\tilde{a}^3A'')$–$HCBr^-(\tilde{X}^2A'')$ photodetachments were carried out on $HCBr^-$ at CCSD(T)/aug-cc-pVQZ level, respectively.

1. Introduction

Recently, the haze weather continues, and this has set the alarm bells ring for human survival [1,2]. Research in the important environment-related molecules are expected to help prevent environmental problems and govern environmental issues, which has been an important research field in molecular physics and chemical physics. Monohalomethylenes (such as HCBr), like the effect of chlorofluorocarbons (CFCs), play an important role in the destruction of the ozone layer [3,4]. In addition, vibrational frequency and IR intensity predictions for HCBr have been investigated via ab initio quantum mechanical methods [5]. Then, Sears and his group produced high-resolution near infrared spectra of HCBr, which invested the geometrical structures and adiabatic transition energy and assigned vibrational and rotational transition [6,7]. Chang recorded the dispersed fluorescence spectra of HCBr $\tilde{A}$–$\tilde{X}$ vibronic transitions and assigned most of the observed vibrational transition [8], which compared with the theoretical calculations done by Yu et al. [7]. And the value of the triplet–singlet energy gap ($2006 \pm 8\ cm^{-1}$) was extracted from the dispersed fluorescence spectra, this will be used to compare with our calculated data.

Many studies have found that the electronic spectroscopy of HCBr is complicated, mainly because a combination of spin–orbit, Renner–Teller effect and Fermi resonance couplings among the different electronic states [9,10]. In order to learn more about their complex relationship, there have been numerous experimental and theoretical reports on the spectroscopic data of the ground and excited electronic states vibrational structure and the singlet–triplet energy gap (ΔE_{ST}) [8,11,12]. For example, fluorescence excited and emission spectra of HCBr in the 450–750 nm region were reported under jet-cooled condition [13]. Kable and his co-works have reviewed previous studies on the spectroscopy and dynamics of halocarbenes: CXY (X = H, F, Cl, Br, I; Y = F, Cl, Br, I), which mainly including the complicated spectroscopy, photochemistry and photophysics dynamics and the singlet–triplet gap of halocarbenes both in theoretical and experimental [14]. Although this system has been extensively invested, there are still need further efforts.

At present, most researches were focus on the neutral molecules HCBr [15–21], and its corresponding negative ion $HCBr^-$ were relatively sparse [22–25]. In 1992, Gilles reported the photoelectron spectra, geometrical structures and corrected adiabatic electron affinity for the singlet state of HCBr [23]. For a change, they proceeded to investigate photoelectron spectra under the 351.1 nm line of an argon ion laser rather than 488 nm, that being the case the higher vibrational levels of triplet states could be researched. And the adiabatic electron affinity for the singlet state of HCBr is found to be 1.454 ± 0.005 eV.

We continued to explore the photoelectron spectra of the $HCBr^-$ theoretically including Duschinsky effects [26]. Geometry

* Corresponding author at: Laboratory of Environment Spectroscopy, Anhui Institute of Optics and Fine Mechanics, Chinese Academy of Sciences, P.O. Box 1125, Hefei 230031, PR China.
** Corresponding author.
E-mail addresses: jliang@mail.ahnu.edu.cn (J. Liang), huangwei@aiofm.ac.cn (W. Huang).

http://dx.doi.org/10.1016/j.cplett.2015.09.021
0009-2614/

optimization and vibrational frequency calculations have been carried out on the $\tilde{X}^2A''$ state of $HCBr^-$, and the $\tilde{X}^1A'$ and $\tilde{a}^3A''$ states of HCBr at different levels. The term energy and electron affinity of HCBr were calculated by the CCSD(T) method with different basis sets and extrapolated to the complete basis set limit (CBS). The geometric structure parameters at the CCSD(T)/aug-cc-pVQZ were exploited in the later spectral simulations. Studies suggest that the theoretical spectra are rather identical to the observed one and the geometry parameters of $HCBr^-$ obtained at CCSD(T)/aug-cc-pVQZ level are accurate.

2. Theoretical method

Calculations of Franck–Condon factors are significant for interpreting vibronic spectra of molecules and investigating nonradiative processes. In order to evaluate the multidimensional Franck–Condon integrals quantitatively, some theoretical methods have been developed in the past several decades. We chose the expanding Hermite polynomials method described by authors [27] for the integrals. An exact expression of Franck–Condon integral $\left\langle \upsilon_1\upsilon_2\upsilon_3 \middle| \upsilon'_1\upsilon'_2\upsilon'_3 \right\rangle$ for the vibronic transition $|\upsilon_1\upsilon_2\upsilon_3\rangle \leftarrow \left|\upsilon'_1\upsilon'_2\upsilon'_3\right\rangle$ has been obtained.

$$\begin{aligned}
\left\langle \upsilon_1\upsilon_2\upsilon_3 \middle| \upsilon'_1\upsilon'_2\upsilon'_3 \right\rangle &= \exp(-\frac{1}{2}K^+\Gamma'K)\exp(C^+AC)N \\
&\times \sum_{k'_{11}=0}^{\upsilon'_1}\sum_{k'_{12}=0}^{\upsilon'_1-k'_{11}}\sum_{k'_{13}=0}^{\upsilon'_1-k'_{11}-k'_{12}}\sum_{k'_{21}=0}^{\upsilon'_2}\sum_{k'_{22}=0}^{\upsilon'_2-k'_{21}}\sum_{k'_{23}=0}^{\upsilon'_2-k'_{21}-k'_{22}}\sum_{k'_{31}=0}^{\upsilon'_3}\sum_{k'_{32}=0}^{\upsilon'_3-k'_{31}}\sum_{k'_{33}=0}^{\upsilon'_3-k'_{31}-k'_{32}} \\
&\times \sum_{k_{11}=0}^{\upsilon_1}\sum_{k_{12}=0}^{\upsilon_1-k_{11}}\sum_{k_{13}=0}^{\upsilon_1-k_{11}-k_{12}}\sum_{k_{21}=0}^{\upsilon_2}\sum_{k_{22}=0}^{\upsilon_2-k_{21}}\sum_{k_{23}=0}^{\upsilon_2-k_{21}-k_{22}}\sum_{k_{31}=0}^{\upsilon_3}\sum_{k_{32}=0}^{\upsilon_3-k_{31}}\sum_{k_{33}=0}^{\upsilon_3-k_{31}-k_{32}} \\
&\times \left\{ \prod_{i-1}^{3}\left[\begin{pmatrix} \upsilon'_i \\ k'_{i1} \end{pmatrix}\begin{pmatrix} \upsilon'_i-k'_{i1} \\ k'_{i2} \end{pmatrix}\begin{pmatrix} \upsilon'_i-k'_{i1}-k'_{i2} \\ k'_{i3} \end{pmatrix} \right.\right. \\
&\times (a'_{i1})^{k'_{i1}}(a'_{i2})^{k'_{i2}}(a'_{i3})^{k'_{i3}} \times H_{\upsilon'_i-k'_{i1}-k'_{i2}-k'_{i3}}(d'_i) \\
&\times \begin{pmatrix} \upsilon_i \\ k_{i1} \end{pmatrix}\begin{pmatrix} \upsilon_i-k_{i1} \\ k_{i2} \end{pmatrix}\begin{pmatrix} \upsilon_i-k_{i1}-k_{i2} \\ k_{i3} \end{pmatrix} \\
&\left.\left. \times (2a_{i1})^{k_{i1}}(2a_{i2})^{k_{i2}}(2a_{i3})^{k_{i3}} \times H_{\upsilon_i-k_{i1}-k_{i2}-k_{i3}}(d_i) \right] \right. \\
&\times \frac{\left[\sum_{i=1}^{3}(k_{i1}+k'_{i1})-1\right]!!}{(2A_1)^{\frac{1}{2}\sum_{i=1}^{3}(k_{i1}+k'_{i1})}}\left(\frac{\pi}{A_1}\right)^{1/2}\frac{\left[\sum_{i=1}^{3}(k_{i2}+k'_{i2})-1\right]!!}{(2A_2)^{\frac{1}{2}\sum_{i=1}^{3}(k_{i2}+k'_{i2})}}\left(\frac{\pi}{A_2}\right)^{1/2} \\
&\left. \times \frac{\left[\sum_{i=1}^{3}(k_{i3}+k'_{i3})-1\right]!!}{(2A_3)^{\frac{1}{2}\sum_{i=1}^{3}(k_{i3}+k'_{i3})}}\left(\frac{\pi}{A_3}\right)^{1/2} \right\}
\end{aligned} \tag{1}$$

with the constraints that $\sum_{i=1}^{3}(k_{i1}+k'_{i1})$, $\sum_{i=1}^{3}(k_{i2}+k'_{i2})$ and $\sum_{i=1}^{3}(k_{i3}+k'_{i3})$ are even. In Eq. (1), Γ' is a 3×3 diagonal matrix of reduced frequency $\omega'_i/\hbar$, and **A** is also a 3×3 diagonal matrix and **C** is a 3×1 vector whose elements and the other coefficients are given in Ref. [27]. Furthermore, from Eq. (1) an exact formula of calculating the three-dimensional overlap integral for the vibronic transition $|\upsilon_1\upsilon_2\upsilon_3\rangle \leftarrow \left|000\right\rangle$, is given explicitly as:

$$\begin{aligned}
\left\langle \upsilon_1\upsilon_2\upsilon_3 \middle| 000 \right\rangle &= \exp\left(-\frac{1}{2}K^+\Gamma'K\right)\exp(C^+AC)N \\
&\times \sum_{k_{11}=0}^{\upsilon_1}\sum_{k_{12}=0}^{\upsilon_1-k_{11}}\sum_{k_{13}=0}^{\upsilon_1-k_{11}-k_{12}}\sum_{k_{21}=0}^{\upsilon_2}\sum_{k_{22}=0}^{\upsilon_2-k_{21}}\sum_{k_{23}=0}^{\upsilon_2-k_{21}-k_{22}}\sum_{k_{31}=0}^{\upsilon_3}\sum_{k_{32}=0}^{\upsilon_3-k_{31}}\sum_{k_{33}=0}^{\upsilon_3-k_{31}-k_{32}} \\
&\times \left\{ \prod_{i=1}^{3}\left[\times \begin{pmatrix} \upsilon_i \\ k_{i1} \end{pmatrix}\begin{pmatrix} \upsilon_i-k_{i1} \\ k_{i2} \end{pmatrix}\begin{pmatrix} \upsilon_i-k_{i1}-k_{i2} \\ k_{i3} \end{pmatrix} \right.\right. \\
&\left.\left. \times (2a_{i1})^{k_{i1}}(2a_{i2})^{k_{i2}}(2a_{i3})^{k_{i3}} \times H_{\upsilon_i-k_{i1}-k_{i2}-k_{i3}}(d_i) \right] \right. \\
&\times \frac{\left[\sum_{i=1}^{3}k_{i1}-1\right]!!}{(2A_1)^{\frac{1}{2}\sum_{i=1}^{3}k_{i1}}}\left(\frac{\pi}{A_1}\right)^{1/2}\frac{\left[\sum_{i=1}^{3}k_{i2}-1\right]!!}{(2A_2)^{\frac{1}{2}\sum_{i=1}^{3}k_{i2}}}\left(\frac{\pi}{A_2}\right)^{1/2} \\
&\left. \times \frac{\left[\sum_{i=1}^{3}k_{i3}-1\right]!!}{(2A_3)^{\frac{1}{2}\sum_{i=1}^{3}k_{i3}}}\left(\frac{\pi}{A_3}\right)^{1/2} \right\}
\end{aligned} \tag{2}$$

with the constraints $\sum_{i=1}^{3}k_{i1}$, $\sum_{i=1}^{3}k_{i2}$ and $\sum_{i=1}^{3}k_{i3}$ all being even.

Furthermore, the Franck–Condon factors (FCFs) of three-dimensional harmonic oscillators including the Duschinsky effect can be evaluated by

$$\mathrm{FCFs} = \left|\left\langle \upsilon_1\upsilon_2\upsilon_3 \middle| \upsilon'_1\upsilon'_2\upsilon'_3 \right\rangle\right|^2 \tag{3}$$

Eq. (1) is exact for harmonic systems, no approximation whatsoever having been introduced in its derivation. This expression should be very useful for studying vibronic spectra and nonradiative processes of molecules.

3. Computational details

Geometry optimization and harmonic vibrational frequency calculations have been carried out on the $\tilde{X}^2A''$ state of $HCBr^-$, and the $\tilde{X}^1A'$ and $\tilde{a}^3A''$ states of HCBr by the B3LYP, QCISD(T), and CCSD(T) levels with several different basis sets (Dunning correlation consistent cc-pVXZ and the augmented correlated consistent polarized valence aug-cc-pVXZ (X = 2, 3 and 4) basis sets. The B3LYP, QCISD(T), and CCSD(T) calculations were performed applying the GAUSSIAN09 suite of programs [28].

We have performed the Franck–Condon factors (FCFs) calculations on the $HCBr(\tilde{X}^1A')$–$HCBr^-(\tilde{X}^2A'')$ and $HCBr(\tilde{a}^3A'')$–$HCBr^-(\tilde{X}^2A'')$ transitions, utilizing CCSD(T)/aug-cc-pVQZ force constants and structures, which involve in the initial electronic state $\tilde{X}^2A''$ of $HCBr^-$, and the final electronic states $\tilde{X}^1A'$ and $\tilde{a}^3A''$ of HCBr. Obviously, spectral simulation methods used and programs employed in the FCF calculations are based on harmonic oscillator models and Duschinsky rotations, which have been described

in Section 2. Then, the computed FCFs were used to simulate the vibrational structures of the $\tilde{X}^1A'$–$\tilde{X}^2A''$ and $\tilde{a}^3A'$–$\tilde{X}^2A''$ photodetachment spectra of $HCBr^-$, employing a GAUSSIAN line-shape and a full-width-at-half-maximum (FWHM) of 340 cm^{-1}.

The term energy and electron affinity were calculated by the CCSD(T) method with different basis sets namely the cc-pVXZ and aug-cc-pVXZ (X = 2, 3 and 4) basis sets. We have exploited the extrapolation procedures, to extrapolate to the complete basis set limit (CBS). The energy obtained at the CBS limit (E_{lim}) by fitting the calculated energies to a simple two-parameter linear fit [29] and a three-parameter mixed GAUSSIAN function [30] of the forms:

$$E(L) = E_{lim} + OL^{-3} \quad (4)$$

$$E(L) = E_{lim} + M\exp[-(L+1)] + N\exp[-(L-1)^2] \quad (5)$$

where L is the maximum angular momentum quantum number in this Letter and E_{lim} is the energy that has extrapolated to the complete basis set limit. When L = 2, 3 and 4, there cc-pVDZ/aug-cc-pVDZ, cc-pVTZ/aug-cc-pVTZ, and cc-pVQZ/aug-cc-pVQZ basis sets, separately. And that O, M and N are adjustable parameters, respectively.

4. Results and discussion

4.1. Geometry optimization and frequency calculations

The optimized geometries and harmonic vibrational frequencies for $\tilde{X}^2A''$ state of $HCBr^-$ and the $\tilde{X}^1A'$ and $\tilde{a}^3A''$ states of HCBr have been showed in Tables 1–3 with the theoretical and/or experimental values available included for comparison. According to the general practice of triatomic molecules, ω_2 represents the bending vibrational frequency [27,31]. And we have designated the C–H stretch as ω_1 and the C–Br stretch as ω_3, respectively.

From Table 1, for the state $\tilde{X}^2A''$ of $HCBr^-$, the bond lengths and angles obtained at several levels are relatively consistent. These results compared with the corresponding available experimental values and previous calculations are also reasonably good agreement. For R(C–H), R(C–Br) and ∠HCBr of $HCBr^-$, the largest deviations between theoretical and experimental bond lengths and angles are less than 0.0397 nm, 0.0367 nm and 4.26°, respectively. The estimated values for the $\tilde{X}^2A''$ of $HCBr^-$ based on ab initio theory at the CCSD(T)/aug-cc-pVQZ level are 1.1195 Å, 2.0633 Å and 95.77°, the difference between the theoretical and experimental values are only 0.0195 Å, 0.0367 Å and 3.23° for R(C–H), R(C–Br) and ∠HCBr, respectively. As noted above, the vibrational frequencies and structures of $HCBr^-$ obtained at CCSD(T)/aug-cc-pVQZ level have showed a good agreement with the experimental values, and therefore were exploited in the later iterative FC analyses and spectral simulations.

For the $\tilde{X}^1A'$ and $\tilde{a}^3A''$ states of HCBr, the computed bond lengths and angles obtained at several different levels of ab initio calculation are highly consistent (Tables 2 and 3). In Tables 2 and 3, it can be seen that the computed values compared well with other theoretical and experimental studies. For the $\tilde{X}^1A'$ states of HCBr, the largest deviations between calculated and experimental bond lengths and angles are less than 0.0363 Å, 0.0054 Å and 1.49° for R(C–H), R(C–Br) and ∠HCBr, respectively [23]. The calculated values of HCBr based on the ab initio method at CCSD(T)/aug-cc-pVQZ level, are 1.1080 Å, 1.8523 Å and 101.13°. The differences between the theoretical and experimental values are only 0.017 Å, 0.0317 Å and 0.87° for R(C–H), R(C–Br) and ∠HCBr, respectively. Still in Table 2, geometrical parameters for the $\tilde{X}^1A'$ state of HCBr at the CCSD(T)/aug-cc-pVQZ results compared with the corresponding available experimental values and other theoretical values are also in a good agreement. Furthermore, for the $\tilde{a}^3A''$ state of HCBr, the computed geometrical parameters and vibrational frequencies obtained at different levels of ab initio calculation are very consistent. However, owing to there is no experimental structural parameters were obtained for comparison, it has been proved that the structural parameters obtained at a higher levels of calculation should be more trustworthy, and therefore the CCSD(T)/aug-cc-pVQZ results were exploited in the later iterative FC analyses and spectral simulations.

4.2. Electron affinity, term energy of HCBr

The electron affinity (EA) and term energy (TE) of HCBr calculated at different levels are listed in Table 4, and it can be concluded that the values at different levels are very regular. The calculated EA values at the CCSD(T)/aug-cc-pVDZ, CCSD(T)/aug-cc-pVTZ and CCSD(T)/aug-cc-pVQZ level are 1.443, 1.458 and 1.483 eV, which match reasonably good with the experimental value [23]. Using basis set extrapolation methods to converge the energies by extrapolating to the complete basis set limit. The calculated EA of HCBr obtained at the basis set limit are 1.499 and 1.480 eV for CCSD(T)/aug-cc-pVXZ using a three-parameter mixed Gaussian function and a simple two-parameter linear fit and they are consistent with the experimental values of 1.454 eV for the electron affinity of HCBr [23]. For the TE of HCBr obtained at CCSD(T)/aug-cc-pVXZ (X = 2, 3 and 4) by using a three-parameter mixed function and a simple two-parameter linear fit extrapolate to the complete basis set limit are 1895.17 and 1909.17 cm^{-1}. These are in excellent agreement with the experimental measurement the term energy of HCBr [8].

4.3. Duschinsky matrix and displacement vector

Upon an electronic transition, the normal coordinates of electronic states generally undergo a displacement distortion as well as a rotation. The rotation results in a mixing of the normal coordinates. Duschinsky [26] (who first studied the normal mode mixing) proposed the transformation between the normal coordinates of the initial (**Q**') and the final (**Q**') electronic states

$$\mathbf{Q}' = \mathbf{J}\mathbf{Q}'' + \mathbf{K} \quad (6)$$

provided that the molecular symmetry remains invariant upon the transition. Here **J** is a constant orthogonal matrix and **K** is a vector whose components are the changes in the nuclear equilibrium positions from the initial to final states. It has been shown that the relationship between the vibrational variables belonging to two different electronic states of a polyatomic molecule is most generally neither linear nor orthogonal [32]. However, in quantitative studies on the FC principle, the linear–orthogonal transformation, Eq. (6), is widely accepted, and in the following discussions, we shall concentrate on this transformation.

The Duschinsky matrix **J** and displacement vector **K** between different electronic states of $HCBr(\tilde{X}^2A'')$–$HCBr^-(\tilde{X}^1A')$ calculated at the CCSD(T)/aug-cc-pVQZ theory level are as follows, respectively:

$$\mathbf{J}^1 = \begin{bmatrix} 0.98 & 0.09 & 0.01 \\ -0.11 & 0.99 & -0.02 \\ -0.02 & 0.02 & 0.98 \end{bmatrix}, \quad \mathbf{K}^1 = \begin{bmatrix} 0.05 \\ 0.09 \\ 2.30 \end{bmatrix} \quad (7)$$

where $\mathbf{K}^1$ are in units of $amu^{1/2}$Å and $\mathbf{J}^1$ describe the mixing of normal modes, reveal that each one of the three a' modes of $HCBr^-$, map on to a linear combination of the three a' modes of HCBr ($\tilde{X}^1A'$). Note that each column in $\mathbf{J}^1$ is normalized, the sum of the squares of the mixing coefficients adding up to unity within rounding errors. The mode mixing matrix $\mathbf{J}^1$ shows that there is some, albeit not large ($J^1_{12} = 0.09$, $J^1_{13} = 0.01$, $J^1_{23} = -0.02$), Duschinsky effect between $\omega_1(a')$, $\omega_2(a')$ and $\omega_3(a')$ vibrational modes. The normal coordinate

Table 1
Summary of the computed and experimental geometric parameters and vibrational frequencies (cm^{-1}) for the $\tilde{X}^2A''$ state of $HCBr^-$ obtained at different levels of calculation.

Method	R(CH)(Å)	R(CBr)(Å)	∠ HCBr(°)	ω_1(CH)	ω_2(bend)	ω_3(CBr)
B3LYP/aug-cc-pVDZ	1.1323	2.1291	95.11	2750	1018	374
B3LYP/aug-cc-pVTZ	1.1177	2.1110	95.36	2780	1036	380
B3LYP/aug-cc-pVQZ	1.1171	2.1052	95.52	2779	1038	383
QCISD(T)/aug-cc-pVDZ	1.1397	2.1348	94.75	2736	1021	373
QCISD(T)/aug-cc-pVTZ	1.1211	2.0804	95.44	2775	1052	408
QCISD(T)/aug-cc-pVQZ	1.1202	2.0638	95.69	2778	1064	420
CCSD(T)/aug-cc-pVDZ	1.1397	2.1326	94.74	2737	1026	375
CCSD(T)/aug-cc-pVTZ	1.1208	2.0789	95.48	2779	1054	411
CCSD(T)/aug-cc-pVQZ	1.1195	2.0633	95.77	2785	1064	421
QCISD(T)/aug-cc-pVTZ[a]	1.126	2.120	94.91			
B3LYP/6-31+G(d)[b]		2.130				
Expt.[c]	1.10	2.10	99.0			393
Expt.[d]						430(40)

[a] Ref.[25].
[b] Ref.[24]
[c] Ref.[23].
[d] Ref.[22].

Table 2
Summary of the computed and experimental geometric parameters and vibrational frequencies (cm^{-1}) for the $\tilde{X}^1A'$ state of HCBr obtained at different levels of calculation.

Method	R(CH) (Å)	R(CBr) (Å)	∠ HCBr(°)	ω_1(CH)	ω_2(bend)	ω_3(CBr)
B3LYP/aug-cc-pVDZ	1.12	1.8792	100.75	2917	1150	667
B3LYP/aug-cc-pVTZ	1.1069	1.8679	101.12	2932	1158	672
B3LYP/aug-cc-pVQZ	1.1067	1.8659	101.15	2929	1159	674
QCISD(T)/aug-cc-pVDZ	1.1273	1.8894	100.51	2894	1146	655
QCISD(T)/aug-cc-pVTZ	1.1103	1.8622	100.83	2923	1152	681
QCISD(T)/aug-cc-pVQZ	1.1087	1.8559	101.00	2934	1155	689
CCSD(T)/aug-cc-pVDZ	1.1269	1.8854	100.64	2898	1149	664
CCSD(T)/aug-cc-pVTZ	1.1101	1.8597	100.99	2925	1152	687
CCSD(T)/aug-cc-pVQZ	1.1080	1.8523	101.13	2941	1156	696
CCSD(T)/aug-cc-pVTZ[a]	1.1102	1.8666	101.00	2926.7	1156.2	682.4
CCSD(T)/6-311++G(3df,pd)[b]	1.110	1.860	101.2	2948	1149	691
MRCI/cc-pVTZ[c]	1.1112	1.8698	101.28	2908.5	1142.6	678.2
B3LYP/6-311++G(3df,2pd)[d]	1.107	1.866	101.13			
Expt.[e]	1.091	1.884	102.0			683
Expt.[f]	1.116(9)	1.854(2)	102.6(9)			
Expt.[g]					1119	676
Expt.[h]		1.85 ± 0.02				
Expt.[i]						670 ± 20

[a] Ref. [17].
[b] Ref. [19].
[c] Ref. [7].
[d] Ref. [20].
[e] Ref. [23].
[f] Ref. [21].
[g] Ref. [8].
[h] Ref. [6].
[i] Ref. [22].

Table 3
Summary of the computed and experimental geometric parameters and vibrational frequencies (cm^{-1}) for the $\tilde{a}^3A''$ state of HCBr obtained at different levels of calculation.

Method	R(CH)(Å)	R(CBr)(Å)	∠ HCBr(°)	ω_1(CH)	ω_2(bend)	ω_3(CBr)
B3LYP/aug-cc-pVDZ	1.0947	1.8294	126.66	3167	898	734
B3LYP/aug-cc-pVTZ	1.0830	1.8184	127.09	3175	898	735
B3LYP/aug-cc-pVQZ	1.0827	1.8165	127.13	3171	898	736
QCISD(T)/aug-cc-pVDZ	1.0992	1.8393	126.49	3171	912	732
QCISD(T)/aug-cc-pVTZ	1.0834	1.8149	126.78	3196	910	752
QCISD(T)/aug-cc-pVQZ	1.082	1.8078	126.90	3205	910	761
CCSD(T)/aug-cc-pVDZ	1.0983	1.8381	126.65	3180	911	734
CCSD(T)/aug-cc-pVTZ	1.0835	1.815	126.81	3195	913	751
CCSD(T)/aug-cc-pVQZ	1.0823	1.8078	126.91	3204	917	762
CCSD(T)/aug-cc-pVDZ[a]	1.0987	1.8403	126.53	3175.0	913.1	731.0
Expt.[b]					994	733

[a] Ref. [17].
[b] Ref. [8].

Table 4
Energies (Hartree) of the $\tilde{X}^2A''$ state of $HCBr^-$ and the $\tilde{X}^1A'$ and $\tilde{a}^3A''$ states of HCBr, as well as the electron affinity (eV) and term energy (cm^{-1}) calculated at different levels. The energy obtained at the complete basis set limit (CBS) by using the extrapolation procedures and the experimental values are also included for comparison.

L	Method	$HCBr^-$	HCBr(s)	HCBr(t)	EA	TE
2	CCSD(T)/aug-cc-pVDZ	−2611.041233	−2610.988217	−2610.980228	1.443	1753.38
3	CCSD(T)/aug-cc-pVTZ	−2611.244780	−2611.191192	−2611.182683	1.458	1867.51
4	CCSD(T)/aug-cc-pVQZ	−2611.324516	−2611.270021	−2611.261426	1.483	1886.38
∞	CBS-3 parameter	−2611.37138	−2611.31629	−2611.30766	1.499	1895.17
	CBS-2 parameter	−2611.35215	−2611.29777	−2611.28907	1.480	1909.17
Expt.					1.454 ± 0.005[a]	2006 ± 8[b]

[a] Ref. [23].
[b] Ref. [8].

displacement $\mathbf{K}^1$ from the anion to the neutral ($\tilde{X}^1A' \leftarrow \tilde{X}^2A''$) are $\Delta Q_1^1 = 0.05$, $\Delta Q_2^1 = 0.09$ and $\Delta Q_3^1 = 2.30$ which correspond to a bond length R(C–H) decrease, a bond angle ∠HCBr increase and a bond length R(C–Br) decrease, respectively. Meanwhile, one can observe that ΔQ_3^1 is much larger than $\Delta Q_1^1/\Delta Q_2^1$, stemming from the large change of the bond length R(C–Br), and therefore a long progression of the stretching vibration (ω_3) transition is shown in the $\tilde{X}^1A' \leftarrow \tilde{X}^2A''$ detachment spectrum of $HCBr^-$ (see the results of the spectral simulation below).

For the $HCBr^-(\tilde{X}^2A'')$–$HCBr(\tilde{a}^3A'')$ electronic transition, the Duschinsky matrix $\mathbf{J}$ and displacement vector $\mathbf{K}$ calculated at the CCSD(T)/aug-cc-pVQZ theory level are as follows, respectively:

$$\mathbf{J}^2 = \begin{bmatrix} -0.85 & 0.50 & -0.01 \\ 0.51 & 0.85 & -0.17 \\ 0.09 & 0.14 & 0.98 \end{bmatrix}, \quad \mathbf{K}^2 = \begin{bmatrix} 0.25 \\ 2.99 \\ 2.12 \end{bmatrix} \tag{8}$$

The normal mode mixing matrix $\mathbf{J^2}$ shows that there is large Duschinsky effect between $\omega_1(a')$ and $\omega_2(a')$ vibrational modes ($J_{12}^2 = 0.50$), whereas vibrational modes $\omega_1(a')$ coupled from $\omega_3(a')$ is small ($J_{13}^2 = -0.01$). From the anion to the neutral ($\tilde{a}^3A'' \leftarrow \tilde{X}^2A''$), the matrix elements of $\mathbf{K^2}$ are $\Delta Q_1^2 = 0.25$, $\Delta Q_2^2 = 2.99$ and $\Delta Q_3^2 = 2.12$, respectively, which correspond to the bond length R(C–H) decrease, the bond angle ∠HCBr increase and the bond length R(C–Br) decrease, respectively. Furthermore, one can observe that $\Delta Q_2^2/\Delta Q_3^2$ is much larger than ΔQ_1^2, due to the large changes of the bond length R(C–Br) and the bond angle ∠HCBr, and therefore long combining progressions of the bending vibration (ω_2) and the stretching vibration (ω_3) transitions are expected in the $\tilde{a}^3A''$–$\tilde{X}^2A''$ detachment spectrum of $HCBr^-$ (see the spectral simulation below).

4.4. Franck–Condon simulations

The simulated stick diagrams of $\tilde{X}^1A'$–$\tilde{X}^2A''$ and $\tilde{a}^3A''$–$\tilde{X}^2A''$ transitions of $HCBr^-$ using the force constants and structures at the CCSD(T)/aug-cc-pVQZ are shown in Figure 1a and b, respectively. The stick diagrams and the simulated spectra of the two detachments merged together with a FWHM of 340 cm^{-1} and a Boltzmann vibrational temperature of 270 K which are showed in Figure 1c (including hot band). In Figure 1a, the C–Br stretching mode ω_3 is involved with the label $(0,0,0)$–$(0,0,n)$ for the transition $(0,0,0)$–$(0,0,\omega_3)$. From the harmonic calculation, it was found that the FCFs for transitions involving the C–H stretching mode ω_1 and the bending mode ω_2 are negligibly small and not included in the assignments. However, the bending mode ω_2 and C–Br stretching mode ω_3 of the $\tilde{a}^3A''$–$\tilde{X}^2A''$ transition are involved in Figure 1b. Also, the labels (0, 0, 0)–$(0,n,0)$, $(0,0,0)$–$(0,n,1)$, and $(0,0,0)$–$(0,n,2)$ correspond to the $(0,0,0)$–$(0,\omega_2,\omega_3)$ transition. It has been found that the bending mode ω_2 and stretching mode ω_3 play a major role. All in all, the $\tilde{X}^1A'$–$\tilde{X}^2A''$ transition for HCBr is mainly a single active vibrational mode (the C–Br stretching mode ω_3), while the $\tilde{a}^3A''$–$\tilde{X}^2A''$ transition appears quite congested due to two active modes (the bending mode ω_2 and C–Br stretching mode ω_3) [23].

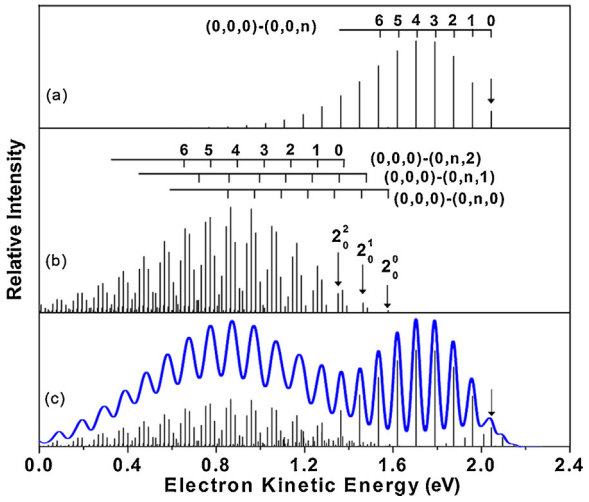

Figure 1. Simulated photoelectron spectra of $HCBr^-$ obtained at a Boltzmann vibrational temperature of 270 K. (a) The simulated stick diagram with vibrational assignments provided for the $\tilde{X}^1A'$–$\tilde{X}^2A''$ detachment process, and (b) the simulated stick diagram with vibrational assignments provided for the $\tilde{a}^3A''$–$\tilde{X}^2A''$ detachment process, and (c) simulated photoelectron spectra with vibrational assignments involved the singlet and triplet detachment processes and with a FWHM of 340 cm^{-1} (including hot band).

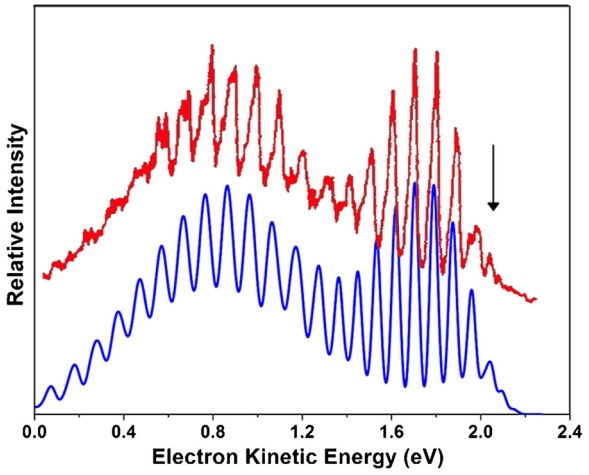

Figure 2. The experimental photoelectron spectra of $HCBr^-$ obtained from Ref. [23] (red line) and the simulated spectra with vibrational assignments provided for the $\tilde{X}^1A'$–$\tilde{X}^2A''$ and $\tilde{a}^3A''$–$\tilde{X}^2A''$ detachment processes with a FWHM of 340 cm^{-1} and a Boltzmann vibrational temperature of 270 K (blue line). (For interpretation of reference to color in this figure legend, the reader is referred to the web version of this article.)

The simulated spectra and the experimental one [23] are shown in Figure 2. Comparing the simulated and the experimental spectra, it was found that the computed photoelectron spectra are nearly perfect to the experimental one. This means for the $\tilde{X}^1A'$–$\tilde{X}^2A''$

and $\tilde{a}^3A''$–$\tilde{X}^2A''$ transitions, the computed geometry changes at the CCSD(T)/aug-cc-pVQZ level are highly accurate, and the harmonic model seems to be reasonably adequate. However, comparing the simulated spectra and the experimental one in Figure 2, it can be seen that reasonably good agreements are obtained mainly for the vibrational peaks with low quantum numbers. Discrepancies between simulation and observation become larger for peaks with higher quantum numbers. This is mainly due to the anharmonicity effects not included in the FCF calculations. Another, in the lower singlet state, Renner–Teller effects shift levels and with a K-dependence and the triplet state has a shallow bending minimum leading to anharmonically spaced bending levels [9,10]. With vibrational quantum numbers increasing, the stronger these effects are and the greater the influence on the simulated spectra.

5. Conclusion

In this study, the geometry optimization and harmonic vibrational frequency calculations were performed on the $\tilde{X}^2A''$ state of $HCBr^-$, and the $\tilde{X}^1A'$ and $\tilde{a}^3A''$ states of HCBr at different methods with different basis sets. Electron affinity and term energy of HCBr were calculated at the CCSD(T) method and extrapolated to the basis set limit. Then, Franck–Condon analyses and spectral simulations were carried out on the $\tilde{X}^1A'$–$\tilde{X}^2A''$ and $\tilde{a}^3A''$–$\tilde{X}^2A''$ photodetachment processes of $HCBr^-$ at CCSD(T)/aug-cc-pVQZ level, using a harmonic model and including Duschinsky effect. The experimental spectra and theoretical one are in good agreement, this show the geometry parameters of $HCBr^-$ obtained at CCSD(T)/aug-cc-pVQZ level are highly accurate and the harmonic model seems to be reasonably adequate.

Acknowledgements

This work was supported by the National Nature Science Foundation of China (No. 21273009), the Nature Science Foundation of the Education Committee of Anhui (No. KJ2009A131), the Program for Innovative Research Team in Anhui Normal University, and the Doctoral Research Foundation of Anhui Normal University (No. 750706).

References

[1] J. Haywood, O. Boucher, Rev. Geophys. 38 (2000) 513.
[2] J. Elm, P. Norman, K.V. Mikkelsen, Phys. Chem. Chem. Phys. 17 (2015) 15701.
[3] J.S. Daniel, S. Solomon, R.W. Portmann, R.R. Garcia, J. Geophys. Res. 104 (1999) 23871.
[4] H.J. Hsu, W.Z. Chang, B.C. Chang, Phys. Chem. Chem. Phys. 7 (2005) 2468.
[5] G.E. Scuseria, M. Duran, R. Maclagan, H.F. Schaefer, J. Am. Chem. Soc. 108 (1986) 3248.
[6] B.C. Chang, T.J. Sears, J. Chem. Phys. 105 (1996) 2135.
[7] H.G. Yu, T. Gonzalez-Lezana, A.J. Marr, J.T. Muckerman, T.J. Sears, J. Chem. Phys. 115 (2001) 5433.
[8] T.C. Tsai, C.W. Chen, B.C. Chang, J. Chem. Phys. 115 (2001) 766.
[9] B.C. Chang, M.L. Costen, A.J. Marr, G. Ritchie, G.E. Hall, T.J. Sears, J. Mol. Spectrosc. 202 (2000) 131.
[10] H.G. Yu, J.T. Muckerman, T.J. Sears, J. Chem. Phys. 116 (2002) 1435.
[11] C.W. Chen, T.C. Tsai, B.C. Chang, J. Mol. Spectrosc. 209 (2001) 254.
[12] C.L. Lee, M.L. Liu, B.C. Chang, Phys. Chem. Chem. Phys. 5 (2003) 3859.
[13] M. Deselnicu, C. Tao, C. Mukarakate, S.A. Reid, J. Chem. Phys. 124 (2006) 134302.
[14] S.H. Kable, S.A. Reid, T.J. Sears, Int. Rev. Phys. Chem. 28 (2009) 435.
[15] S.L. Xu, K.A. Beran, M.D. Harmony, J. Phys. Chem. 98 (1994) 2742.
[16] M. Schwartz, P. Marshall, J. Phys. Chem. A 103 (1999) 7900.
[17] D.A. Dixon, W.A. de Jong, K.A. Peterson, J.S. Francisco, J. Phys. Chem. A 106 (2002) 4725.
[18] B.C. Chang, J. Guss, T.J. Sears, J. Mol. Spectrosc. 219 (2003) 136.
[19] Z. Li, J.S. Francisco, J. Chem. Phys. 109 (1998) 134.
[20] S. Burrill, F. Grein, Can. J. Phys. 86 (2008) 1333.
[21] A.J. Marr, S.W. North, T.J. Sears, L. Ruslen, R.W. Field, J. Mol. Spectrosc. 188 (1998) 68.
[22] K.K. Murray, D.G. Leopold, T.N. Miller, W.C. Lineberger, J. Chem. Phys. 89 (1988) 5442.
[23] M.K. Gilles, K.M. Ervin, J. Ho, W.C. Lineberger, J. Phys. Chem. 96 (1992) 1130.
[24] M.L. McKee, J. Org. Chem. 62 (1997) 7942.
[25] J.X. Liang, Y.B. Wang, Z.Y. Geng, G.H. Li, Y.J. Wei, Struct. Chem. 24 (2013) 455.
[26] F. Duschinsky, Acta Physicochim. URSS 7 (1937) 551.
[27] J. Liang, F. Cui, R. Wang, W. Huang, Z. Cui, J. Mol. Spectrosc. 286 (2013) 12.
[28] M.J. Frisch, G.W. Trucks, H.B. Schlegel, G.E. Scuseria, M.A. Robb, J.R. Cheeseman, G. Scalmani, V. Barone, B. Mennucci, G.A. Petersson, Gaussian, Gaussian Inc., Wallingford, CT, 2009.
[29] W. Klopper, K.L. Bak, P. Jorgensen, J. Olsen, T. Helgaker, J. Phys. B: At. Mol. Opt. phys 32 (1999) R103.
[30] K.A. Peterson, D.E. Woon, T.H. Dunning, J. Chem. Phys. 100 (1994) 7410.
[31] R. Li, X. Zhang, H. Zheng, J. Liang, Z. Cui, J. Mol. Struct. (THEOCHEM) 860 (2008) 106.
[32] I. Ozkan, J. Mol. Spectrosc. 139 (1990) 147.